# Effect of wave skewness and sediment particle size on sediment transport due to combined wave–current seabed boundary layer streaming

Mohammad Saud Afzal*[1], Lars Erik Holmedal[2], and Dag Myrhaug[3]

[1]Asst. Professor, Indian Institute of Technology, Kharagpur, India, Email: saud@civil.iitkgp.ac.in

[2]Professor, Department of Marine Technology, Norwegian University of Science and Technology, Trondheim, Norway, Email: lars.erik.holmedal@ntnu.no

[3]Professor Emeritus, Department of Marine Technology, Norwegian University of Science and Technology, Trondheim, Norway, Email: dag.myrhaug@ntnu.no

## ABSTRACT

The effect of wave skewness and sediment particle size on near-bed sediment dynamics and transport owing to wave-induced streaming is examined in this study. Here, wave-dominated flow over a flat rough bed is studied, with wave propagation forming a non-zero angle with the current. It is observed that the increase in wave skewness, increases the mean sediment transport, which is consistent with prior findings for the particular situation of horizontally uniform Stokes forcing. The mean sediment transport beneath combined second ($2^{nd}$) order Stokes waves and current has been investigated for fine, medium and coarse sand, respectively. Due to inertia both the mean bedload vector and the depth-integrated suspended flux vector are less rotated (relative to the wave propagation direction) for coarse sand than for fine sand. The mean bedload transport is largest for coarse sand while the mean suspended sediment transport is largest for fine sand.

## INTRODUCTION

In nature, the movement of the particles near the seabed is affected by the presence of both waves and current. The main part of the interaction between the particles and the water takes place within the seabed boundary layer. A rough approximation of the boundary layer thickness is given by $\delta = \sqrt{\nu_t T}$ where $\nu_t$ is the eddy viscosity and $T$ is the time period of the flow. The characteristic time scale associated with the waves is much smaller than that associated with the currents in the sea, leading to the wave-induced boundary layers being much thinner than bottom current boundary layers which again results in in much larger shear stresses across the wave bottom boundary layer. The thickness of current boundary layers often covers a substantial part of the water depth while the wave boundary layer thickness is typically less than 25 cm (Nielsen, 1992).

The physical mechanisms affecting this movement includes the classical wave-current interaction and two competing streaming mechanisms as discussed in detail by Afzal et al. (2015). The interaction between the horizontal and vertical velocity components beneath progressive waves yields a wave-averaged depth varying force leading to a small drift in the wave propagation direction. This mechanism is termed as Longuet-Higgins streaming (Longuet-Higgins, 1953) and has been studied in detail by van Rijn et al. (2007); Holmedal and Myrhaug (2009); Kranenburg et al. (2012); Holmedal et al. (2013); Fuhrman et al. (2013); Afzal et al. (2015). The non-linearity (as in skewed waves) of the wave (as present in $2^{nd}$ order Stokes waves and other higher order waves) induces another type of seabed boundary layer streaming denoted as streaming due to wave skewness. This is due to asymmetry in turbulence of successive wave half-cycles under skewed waves, which forces the flow in the opposite direction of wave propagation. This streaming mechanism was investigated experimentally by Ribberink and Al-Salem (1995); Yuan and Madsen (2015) and numerically by Davies and Li (1997); Scandura (2007) for horizontally uniform flow with skewed forcing, by Holmedal and Myrhaug (2009) for $2^{nd}$ order progressive waves and by Holmedal et al. (2013) for collinear waves and current, and subsequently by Afzal et al. (2015) for progressive waves with an arbitrary angle of attack on the current. The latter part of the study elaborates the classical wave-current interaction mechanism and two competing streaming mechanisms, which influence the direction and veering of the resultant current, which is difficult to measure in either large wave flume or in closed channels. Some other works (An et al., 2011; Rajaratnam et al., 1988) include the study of steady streaming around structures due to oscillatory and steady flows.

Sediment transport at the seabed owing to wave-current interaction and streaming mechanisms have also long been studied using both experiments and numerical techniques, including the laboratory experiments conducted by Ribberink et al. (2000); Dohmen-Janssen et al. (2001); Dohmen-Janssen and Hanes (2002); Schretlen et al. (2011); Bose and Dey (2014), and Ali and Dey (2016). Numerical simulations are reported by Hsu et al. (2004); McAnally et al. (2007); Ruessink et al. (2009); Holmedal and Myrhaug (2009); Fuhrman et al. (2009); Yu et al. (2010); Ruessink et al. (2011); van der A et al. (2011); Fuhrman et al. (2013), and Kranenburg et al. (2013). The most recent work investigating sediment transport owing to streaming is that by Afzal et al. (2021) who used numerical simulations to examine the affect of wave-induced streaming, non-linear wave-forcing and wave-current interaction on the near-bed sediment dynamics and transport. These numerical studies were performed on wave-dominated flow over a flat rough bed, where the waves propagate at a non-zero angle relative to the current. They validated their numerical model with the experimental results of Dohmen-Janssen et al. (2001), and Dohmen-Janssen and Hanes (2002) for an oscillating water tunnel and large scale flume respectively. In the present work, it is investigated how the wave skewness and the sediment particle size affects the near-bed sediment dynamics and transport due to streaming for wave-dominated wave-current flows. This work is an extension of the study performed by Afzal et al. (2021).

## NUMERICAL MODEL

The numerical model of the boundary layer flow over a rough bed near ocean bottom (fixed at $z = z_0 = k_N/30$, where $k_N$ is the equivalent Nikuradse roughness) as presented in Afzal et al. (2021) is used in this study and thus only salient features of the hydrodynamics and sediment transport model formulations are presented here. The definition sketch of the problem is shown in Figure 1.

The governing equations for flow hydrodynamics include the Reynolds-averaged boundary layer momentum and continuity equations and the modified $k$-$\epsilon$ model for turbulence closure as given below:

$$\frac{\partial u}{\partial t} + u\frac{\partial u}{\partial x} + v\frac{\partial u}{\partial y} + w\frac{\partial u}{\partial z} = -\frac{1}{\rho}\frac{\partial p}{\partial x} + \frac{\partial}{\partial z}(\nu_T\,\frac{\partial u}{\partial z}) \tag{1}$$

$$\frac{\partial v}{\partial t} + u\frac{\partial v}{\partial x} + v\frac{\partial v}{\partial y} + w\frac{\partial v}{\partial z} = -\frac{1}{\rho}\frac{\partial p}{\partial y} + \frac{\partial}{\partial z}(\nu_T\,\frac{\partial v}{\partial z}) \tag{2}$$

$$\frac{\partial u}{\partial x} + \frac{\partial v}{\partial y} + \frac{\partial w}{\partial z} = 0 \tag{3}$$

where $u$, $v$ and $w$ are the components of velocity in $x$,$y$ and $z$-direction respectively. Here, $p$ is the pressure, and $\rho$ is the density of water.

$$\frac{\partial k}{\partial t} + u\frac{\partial k}{\partial x} + v\frac{\partial k}{\partial y} + w\frac{\partial k}{\partial z} = \frac{\partial}{\partial z}(\,\frac{\nu_T}{\sigma_k}\frac{\partial k}{\partial z}\,) + \nu_T\,((\,\frac{\partial u}{\partial z}\,)^2 + (\,\frac{\partial v}{\partial z}\,)^2) - \epsilon - B \tag{4}$$

$$\frac{\partial \epsilon}{\partial t} + u\frac{\partial \epsilon}{\partial x} + v\frac{\partial \epsilon}{\partial y} + w\frac{\partial \epsilon}{\partial z} = \frac{\partial}{\partial z}(\,\frac{\nu_T}{\sigma_\epsilon}\frac{\partial \epsilon}{\partial z}\,) + c_{\epsilon 1}\frac{\epsilon}{k}\nu_T\,((\,\frac{\partial u}{\partial z}\,)^2 + (\,\frac{\partial v}{\partial z}\,)^2) - c_{\epsilon 2}\frac{\epsilon^2}{k} - c_{\epsilon 3}\frac{\epsilon}{k}B \tag{5}$$

where $k$ is the turbulent kinetic energy, $\epsilon$ is the turbulent dissipation rate, and $B = N^2\nu_T/\sigma_p$ is the buoyancy flux. The Brunt-Vaisala frequency $N$ is $\sqrt{-g/\rho_t\frac{\partial \rho_t}{\partial z}}$ and $\rho_t = s\rho c + \rho(1-c)$ is the fluid-sediment density. Here, the acceleration due to gravity is given by $g$, the specific gravity $s$ and the sediment concentration by $c$.

As specified by Nielsen (1992), the governing equations for $\Phi$ (instantaneous dimensionless bedload transport) in terms of the Shields parameter $\Theta$ is presented as

$$\Phi = 12\Theta^{\frac{1}{2}}(\Theta - \Theta_c)\,\frac{\Theta}{\mid \Theta \mid} \tag{6}$$

where

$$\Phi = \frac{q_b}{(g(s-1)d_{50}^3)^{\frac{1}{2}}} \tag{7}$$

$$\Theta = \frac{\tau_{\mathrm{b}}}{\rho g(s-1)d_{50}} \tag{8}$$

Here, $q_b$ is the instantaneous dimensional bedload transport, $\tau_{\mathrm{b}}$ is the dimensional instantaneous sea bed shear stress, $d_{50}$ is the median grain size diameter of specific gravity ($s$) equal to 2.65 for quartz sand. Recently, (Sui et al., 2021, Eq. 3) have derived a more accurate formula for the critical Shields parameter under assumption of steady currents only. They derived this formula by fitting a curve to the modified Shields diagram curve reported in Yalin and Karahan (1979). However, the formula's application to combined wave-current flows has yet to be validated. Therefore, in the present study a simpler approach has been taken, where bedload transport occurs when the critical Shields parameter is greater than $\Theta_c = 0.05$.

The governing equation for calculating $c$ (sediment concentration) $c$ is specified as :

$$\frac{\partial c}{\partial t} + u\frac{\partial c}{\partial x} + v\frac{\partial c}{\partial y} + w\frac{\partial c}{\partial z} = \frac{\partial (w_s c)}{\partial z} + \frac{\partial}{\partial z}(\epsilon_s \frac{\partial c}{\partial z}) \tag{9}$$

$$\epsilon_s = \nu_T + \nu \tag{10}$$

The addition of $\nu$ to the sediment diffusivity $\epsilon_s$ in Eq. 9 is done to improve the numerical model's stability. In principle addition or removal of $\nu$ does not make any difference in the values of suspended sediment concentration owing to the turbulent nature of the flow (i.e. $\nu \ll \nu_t$).

The boundary layer approximation has been utilised to obtain Eq. 9. Here, $\mathrm{w}_s$ (settling velocity of sediments) is taken from van Rijn (1993) in conjunction with the hindered settling correction as given by Richardson and Zaki (1954). The diffusivity of the sediment is given by $\epsilon_s$ is and the kinematic viscosity of water by $\nu$.

The permanent wave form approximation (Eqs. 11 and 12) which minimizes the three-dimensional boundary layer equation to spatially one-dimensional equation (see e.g. Afzal et al., 2015, 2020) is used to simplify Eqs. (1) - (5) and Eq. (9).

The permanent wave form simplification for a flow quantity $\phi$ beneath linear and a $2^{nd}$ order Stokes wave is given as

$$\frac{\partial \phi}{\partial x} = -\frac{cos\theta}{c_p}\frac{\partial \phi}{\partial t} \tag{11}$$

$$\frac{\partial \phi}{\partial y} = -\frac{sin\theta}{c_p}\frac{\partial \phi}{\partial t} \tag{12}$$

Here, $\theta$ is the angle between the waves and the current.

It appears that for wave dominated flows, the permanent wave form approximation works well, as will be shown later in this note by comparisons with laboratory measurements. Since the bed is considered hydraulically rough where the viscous sub-layer is absent, a no-slip condition is utilized. The boundary conditions for turbulent quantities ($k$ and $\epsilon$) are presented (Rodi, 1993) using a logarithmic velocity profile. The Zyserman and Fredsøe (1994) formula is used to obtain the reference sediment concentration:

$$c_a = \frac{0.331\,(\,\Theta - \Theta_c\,)^{1.75}}{1 + 0.720\,(\,\Theta - \Theta_c\,)^{1.75}} \quad \text{at} \quad z = z_a = 2\,d_{50} \tag{13}$$

The velocity at the top (located at $z = z_{max}$) of the boundary layer is given as:

$$u = U_{00}\,\cos\theta + U_c \tag{14}$$

$$v = U_{00}\,\sin\theta \tag{15}$$

where $U_{00}$ is the horizontal near-bed wave velocity component which is calculated using the $2^{nd}$ order Stokes theory (Dean and Dalrymple, 1991) as below .

$$
\begin{aligned}
U_{00}(x,y,z,t) = \quad & \pm a \frac{g k_p}{\omega} \frac{\cosh(k_p z)}{\cosh(k_p h)} \cos(\, k_p x \, cos\theta + \, k_p y \, sin\theta - \omega t) \\
\pm \quad & \frac{3}{4} \frac{a^2\, \omega k_p \cosh(2k_p z)}{\sinh^4(k_p h)} \cos 2(\, k_p x \, cos\theta + \, k_p y \, sin\theta - \omega t) \\
W_{00}(x,y,z,t) = \quad & \pm a \frac{g k_p}{\omega} \frac{\sinh(k_p z)}{\cosh(k_p h)} \sin(\, k_p x \, cos\theta + \, k_p y \, sin\theta - \omega t) \\
\pm \quad & \frac{3}{4} \frac{a^2\, \omega k_p \sinh(2k_p z)}{\sinh^4(k_p h)} \sin 2(\, k_p x \, cos\theta + \, k_p y \, sin\theta - \omega t)
\end{aligned}
\tag{16}
$$

where $W_{00}$ is the vertical near-bed wave velocity component.

As previously discussed in Afzal et al. (2015, paragraph 3.4), The wave-current boundary layer models (one-dimensional) must be coupled at a vertical location within a sheared layer for the boundary layer approximation (implying hydrostatic pressure) to hold. This modelling approach can only be justified if the predicted seabed boundary layer velocity, sediment flux and sediment concentration remain independent of $z_{max}$ (as long as $z_{max}$ is chosen such that the boundary layer approximation holds). This has been tested here for $A/k_N = 1800$ (where A is the near-bottom wave excursion amplitude and $k_\mathrm{N} = 2.5\, d_{50}$), $U_c = 0.1$ m/s and $d_{50} = 0.21$ mm by first extrapolating the mean velocity profile obtained from $z_{max}$=0.25m up to 0.50m above the bottom and then re-doing the simulation with $z_{max} = 0.50$m using the extrapolated velocity as a Dirichlet condition there. Figure 2 represents the predicted mean velocity profiles, suspended sediment flux profiles and the sediment concentration profiles, for opposing and following waves and current, obtained for both $z_{max} = 0.25$m and $z_{max} = 0.50$m. It is observed that the velocity profiles are almost identical up to about 12 cm above the bed; the mean sediment flux and sediment concentration profiles are also almost identical. This confirms that the used methodology yields consistent mean velocity profiles near the bed, and that the mean suspended sediment flux and the mean sediment concentration profiles remain nearly the same independent of the value of the $z_{max}$.

Zero flux conditions (Fuhrman et al., 2010) for the turbulent quantities ($k$ and $\epsilon$) are applied as

$$\frac{\partial k}{\partial z} = 0 \tag{17}$$

$$\frac{\partial \epsilon}{\partial z} = 0 \tag{18}$$

Further, zero flux condition (Eq. 19) is applied to calculate the concentration of sediment particles at top of the boundary layer i.e. at $z = z_{max}$.

$$\nu_T \frac{\partial c}{\partial z} + \mathrm{w}_s\, c = 0 \tag{19}$$

As shown by Fredsøe et al. (1985), Eq. (19) degenerates to .

$$c \to 0 \quad when \quad z \to \infty \tag{20}$$

The horizontal pressure gradient due to the application of boundary layer approximation is assumed constant and calculated using the equations below.

$$-\frac{1}{\rho}\frac{\partial p}{\partial x} = \frac{\partial U_0}{\partial t} + U_0\frac{\partial U_0}{\partial x} + V_0\frac{\partial U_0}{\partial y} - \frac{1}{\rho}\frac{\partial p_c}{\partial x} \tag{21}$$

$$-\frac{1}{\rho}\frac{\partial p}{\partial y} = \frac{\partial V_0}{\partial t} + U_0\frac{\partial V_0}{\partial x} + V_0\frac{\partial V_0}{\partial y} - \frac{1}{\rho}\frac{\partial p_c}{\partial y} \tag{22}$$

where

$$U_0 = U_{00}\,\cos\theta,\;\; V_0 = U_{00}\,\sin\theta,\;\; W_0 = W_{00} \tag{23}$$

where $\partial p_c/\partial x$ is the constant pressure gradient owing to the current in $x$- direction whereas $\partial p_c/\partial y$ is the corresponding pressure gradient in $y$- direction. It is important to note that here the wave-current boundary layer is forced by a prescribed motion at a given distance from the bottom, and that this implies that the two-way coupling between the flow inside and outside the predicted wave-current boundary layer is not considered. Despite this weakness, the present approach yields reliable predictions of both the near-bed wave-current velocity (i.e., about the first 15 cm above the seabed) and the near-bed suspended sediment concentration, as will be shown later in Fig. 2. This has also been demonstrated previously in Afzal et al. (2021; Figs. 2 and 3) showing successful comparisons between predictions and laboratory measurements.

The governing equations are solved using $2^{nd}$ order central finite difference method in space with a geometric stretching factor of 1.09 near the bed. Here 100 vertical grid cells are used to resolve the boundary layer as discussed in Afzal et al. (2021, 2015); Holmedal et al. (2013); Holmedal and Myrhaug (2009). Previous studies have shown that the grid resolution adopted in the study is adequate for obtaining grid independent results leading to accurate prediction of the seabed shear stress (Holmedal et al., 2003, Fig. 5). The turbulent quantities ($k$ and $\epsilon$) are stored using a vertical staggered arrangement at the boundary of the velocity $u$ cells. Present study used a spin-up time of 800 wave periods; sufficient for establishing a fully developed flow. However, the simulations were run for 6400 additional wave periods to check the sufficiency of the adopted spin-up time. Further details of the numerical set up and simulation settings are given in Afzal et al. (2021).

### Validation

This is a technical note representing an extension of already published work (Afzal et al., 2021). The code used in the present work has been extensively validated in series of papers. For instance, Afzal et al. (2021, 2015) validated the code for sediment transport and hydrodynamics, respectively, beneath combined wave-current flows where waves form an arbitrary angle with the current. The present code has also been validated against experiments in Holmedal et al. (2004).

## RESULTS AND DISCUSSION

Afzal et al. (2015) performed simulations to investigate the impact of streaming on seabed boundary layer velocities when waves propagates at a non-zero angle to the current. They observed that the mean velocity profile displays a veering tendency that is heavily influenced by streaming in wave-dominated conditions. They reported that the influence of streaming decreases on the boundary layer of flow as the flow becomes less wave dominated. The streaming in such cases (mostly current dominated case) still affects the veering of the mean velocities. They also found that the increase in bottom roughness, decreases the mean velocity in the direction of current whereas the velocity perpendicular to the current direction increases. The work by Afzal et al. (2015) was followed by Afzal et al. (2021) who used numerical simulations to examine the affect of wave-induced streaming on sediment transport for wave dominated flows over a flat rough bed. They validated their numerical model with the experimental results of Dohmen-Janssen et al. (2001), and Dohmen-Janssen and Hanes (2002) for an oscillating water tunnel and a large scale flume respectively. They observed that the mean sediment transport (both bedload and suspended flux) is oriented along the direction of wave propagation for collinear waves and current case, with the maximum sediment transport occurring beneath $2^{nd}$ order Stokes waves. For non-collinear waves and current, an increase of $\theta$ reduces the mean sediment transport. For a given $\theta$, the maximum sediment transport occurs under $2^{nd}$ order Stokes waves, followed by linear propagating waves, horizontally uniform Stokes forcing, and minimum for horizontally uniform linear forcing. Furthermore, due to the current, the mean sediment transport direction vector (for both bedload and suspended flux) is rotated towards the right of the wave propagation direction which is largest for horizontally uniform linear forcing, followed by horizontally uniform Stokes forcing, linear propagating waves and $2^{nd}$ order Stokes waves.

In the present work (continuation of Afzal et al. (2021)) the effect of wave skewness and the sediment particle size on the sediment transport due to streaming is studied for realistic wave and current conditions. The ocean surface waves amplitude is chosen to be $a$=1.22 m with wave periods of 6, 8, 10 and 12 s. The current velocity $U_c$ = 0.1 m/s is specified at $z_{max}$ = 0.25 m above the bed. The angle $\theta$ between the waves and the current varies from $0^o$ to $180^o$; the flow depth is 8 m and the wave length is 45 m. Furthermore, the median sand grain diameters chosen are $d_{50}$ = 0.13, 0.21, 0.32 mm corresponding to fine, medium and coarse grains, respectively. The flow parameters and sediment sizes used in the present study are identical to the study performed by Dohmen-Janssen et al. (2001) and Dohmen-Janssen and Hanes (2002).

## Effect of wave skewness on the mean sediment transport beneath waves and current

The impact of wave skewness on wave-averaged (mean) sediment transport is explored in this study. Four different wave period $T_p$ (6,8,10,12 s) are chosen while keeping all the other physical parameters (water depth, wave amplitude and the current speed) constant. The wave skewness factor $R$ is defined as

$$R = \frac{U_{wc}}{U_{wc} + U_{wt}} \tag{24}$$

where $U_{wc}$ and $U_{wt}$ are the crest and the trough velocity outside the boundary layer, respectively. For $T_p$= 6 s, R is 0.53 and increases to 0.58 for $T_p$= 12 s; see Table 1. The effect of increasing the wave period $T_p$ on sea bed boundary layer flow is discussed in detail in Afzal et al. (2015) and in Holmedal and Myrhaug (2009). They discussed that on increasing $T_p$ (keeping constant all the other physical parameters) results in two different effect on the flow. On increasing $T_p$, the wave velocity amplitude decreases which results in smaller streaming-induced velocities (the wave velocity amplitude is proportional to $a\omega = 2 * \pi * a/T$. Since a is constant, increasing $T_p$ will imply a smaller wave velocity and hence a smaller streaming induced velocity). This leads to a reduced wave velocity component compared to the current resulting in a more current-dominated flow. Second, a larger $T_p$ results in a larger wave length and therefore $k_p h$ decreases. This implies shallower water conditions finally leading to an increased wave skewness factor $R$. It is important to note that isolating the effect of wave skewness and that of changing $k_p h$ is not possible. We can however isolate the effects of wave skewness and viscous streaming by using different wave forcing.

Fig. 3 represents the mean magnitude and direction of the mean bedload transport $\overline{q}_{bt}$ beneath $2^{nd}$ order Stokes waves and current for $\theta$= $45^o$, $90^o$ and $135^o$. The direction of bedload transport is shown by solid lines vectors, whereas direction of wave propagation is represented by dashed lines vectors. Fig. 3 shows that i) the increase in the angle between waves and current causes a decrease in mean bedload transport, and ii) the mean bedload transport $\overline{q}_{bt}$ increases as $Tp$ increases due to increased wave skewness for a given angle $\theta$. Overall the bedload transport is in the direction of wave propagation. A closer inspection as can be seen from Fig. 4, however, it reveals that the bedload transport is rotated slightly right to the wave propagation due to the current and this rotation is largest for $T_p$ = 6s and smallest for $T_p$ = 12s. The largest wave period yields the largest bedload transport in the direction of wave propagation (due to the largest wave skewness) and thus the smallest rotation of the bedload transport vector to the right. However This effect is very small.

Fig. 5 represents the magnitude and direction of the mean wave-averaged suspended sediment transport $\int_{z_0}^{z_{max}} \overline{Uc}dz$ beneath $2^{nd}$ order Stokes waves and current corresponding to the conditions in Fig. 3. The direction of mean suspended transport is shown by solid line vectors, whereas the direction of wave propagation is represented by dashed lines vectors. The increase in angle between the waves and current decreases the mean suspended sediment transport, and the increase in $T_p$ increases the $\int_{z_0}^{z_{max}} \overline{Uc}dz$ for a specific angle $\theta$ Similar to the bedload transport, the suspended sediment transport is overall in the direction of wave propagation, although a closer inspection as can be seen from Fig.6 reveals that it is directed slightly right to the direction of wave propagation due to the current. The increased wave skewness (as $T_p$ increases) leads to an enhancement of the suspended sediment transport in the wave propagation direction, leading to $\int_{z_0}^{z_{max}} \overline{Uc}dz$ being least rotated relative to the wave propagation direction for $T_p$ = 12 s; the rotation increases as $T_p$ decreases. As for the bedload transport shown in Fig. 3, this effect is very small.

**Effect of median sand grain diameter on the mean sediment transport beneath waves and current**

In the forthcoming the settling velocities $w_s$ = 0.0119 m/s for $d_{50}$ = 0.13 mm, $w_s$ = 0.026 m/s for $d_{50}$ = 0.21 mm and $w_s$ = 0.030 m/s for $d_{50}$ = 0.32 mm have been applied ; these values yield good predictions of measurements, as demonstrated in (Afzal et al., 2015, Fig. 2). Fig. 7 represents the magnitude and direction of the mean bedload transport $\overline{q}_{bt}$ beneath $2^{nd}$ order Stokes waves and current for $d_{50}$ = 0.32, 0.21 and 0.13 mm and for $\theta$= 45$^o$, 90$^o$ and 135$^o$ for $T_p$ = 6s. The direction of bedload transport is shown by solid lines vectors, whereas the direction of wave propagation (given for comparison) is represented by dashed lines vectors. Fig. 7 shows that for the present case $\overline{q}_{bt}$ decreases as $d_{50}$ decreases. It appears (Fig. 8) that, at least for 90$^o$ and 135$^o$, $\overline{q}_{bt}$ is least rotated for $d_{50}$ = 0.32 mm, more rotated for $d_{50}$ = 0.21 mm, and most rotated for $d_{50}$ = 0.13 mm, although these differences are very small. This is due to inertia; larger grains lead to a smaller rotation of the bedload transport vector towards the current direction relative to smaller grains.

Fig. 9 represents the magnitude and direction of the wave-averaged suspended sediment transport $\int_{z_0}^{z_{max}} \overline{Uc}dz$ beneath 2$^{nd}$ order Stokes waves and current corresponding to the conditions discussed in Fig. 7. Here, the direction of mean suspended transport is shown by solid line vectors, whereas the direction of wave propagation is represented by dashed lines vectors.As expected, $\int_{z_0}^{z_{max}} \overline{Uc}dz$ increases as $d_{50}$ decreases; similar results were found by Holmedal and Myrhaug (2009) for sediment transport beneath 2$^{nd}$ order Stokes waves. Due to inertia, $\int_{z_0}^{z_{max}} \overline{Uc}dz$ is least rotated for $d_{50}$ = 0.32 mm, more rotated for $d_{50}$ = 0.21 mm, and most rotated for $d_{50}$ = 0.13 mm. These differences as seen from Fig. 10, however, are very small.

Table 2 shows the range of the maximum Shields number ($\Theta_{max}$) and the minimum Rouse number $Z_{min}$ (a non-dimensional number which determines if the sediment will be transported as either bedload, suspended load or wash load) during a wave-cycle for waves plus current beneath 2$^{nd}$ order propagating Stokes waves for $d_{50}$ = 0.32, 0.21 and 0.13 mm; for $\theta$= 45$^o$, 90$^o$ and 135$^o$. Here, $\Theta_{max}$ is always larger than 0.8 (approximately equal to 0.8 for $d_{50}$ = 0.32 mm) which implies that the bottom sediment transport takes place as sheet flow. The lower limit of $\Theta_{max}$ corresponds to $\theta$ = 180$^o$ whereas the upper limit corresponds to $\theta$ = 0$^o$ for all three sand grain diameters. Furthermore, the values of $Z_{min}$ indicate that the sediment transport takes place both as suspended load and bedload ($Z_{min}$ > 0.8). For $d_{50}$ = 0.13 mm, the values of $Z_{min}$ indicates that the sediments will also be transported as washload ($Z_{min}$ < 0.8) which is considered as sheet flow in the present numerical model.

## CONCLUSIONS

In the present work, it is investigated how the wave skewness and the sediment particle size affect the near-bed sediment dynamics and transport due to streaming for wave dominated flows where the wave propagation forms a non-zero angle with the current. Here flow over a flat rough bed is considered. It is shown that the increase in wave skewness increases the mean sediment transport which is consistent with previous results obtained by e.g. Fuhrman et al. (2009) for the special case of horizontally uniform Stokes forcing. Furthermore, the effect of the median sand grain diameter on the mean sediment transport has been examined by predicting the mean sediment transport beneath $2^{nd}$ order Stokes waves for fine, medium, and coarse sand, respectively. Due to inertia both the mean bedload vector and the depth-integrated suspended flux vector are less rotated (relative to the wave propagation direction) for coarse sand than for fine sand. The mean bedload transport is largest for coarse sand while the mean suspended sediment transport is largest for fine sand.

### Data Availability Statement

All data, models, or code that support the findings of this study are available from the corresponding author upon reasonable request.

### Acknowledgements

This work was carried out mainly as a part of the strategical university program "Air-Sea Interaction and Transport Mechanisms in the Ocean", funded by the Norwegian Research Council. Further work was supported by Early Carrier Research Award titled "Large Scale CFD modelling of hydrodynamics and scour around offshore wind farms", funded by the Science and Engineering Research Board (SERB), Department of Science and Technology, India. The grant number is ECR/2018/000284. Both the supports are gratefully acknowledged.

## REFERENCES

Afzal, M. S., Holmedal, L. E., and Myrhaug, D. (2015). "Three-dimensional streaming in the seabed boundary layer beneath propagating waves with an angle of attack on the current." *Journal of Geophysical Research: Oceans*, 4370–4391.

Afzal, M. S., Holmedal, L. E., and Myrhaug, D. (2021). "Sediment transport in combined wave-current seabed boundary layers due to streaming." *Journal of Hydraulic Engineering*, 147(4), 04021007.

Ali, S. Z. and Dey, S. (2016). "Theory of turbulent flow over a wavy boundary." *Journal of Hydraulic Engineering*, 142(6), 04016006.

An, H., Cheng, L., and Zhao, M. (2011). "Steady streaming around a circular cylinder near a plane boundary due to oscillatory flow." *Journal of Hydraulic Engineering*, 137(1), 23–33.

Bose, S. K. and Dey, S. (2014). "Gravity waves on turbulent shear flow: Reynolds averaged approach." *Journal of Hydraulic Engineering*, 140(3), 340–346.

Davies, A. G. and Li, Z. (1997). "Modelling sediment transport beneath regular symmetrical and asymmetrical waves above a plane bed." *Continental Shelf Research*, 17(5), 555–582.

Dean, R. G. and Dalrymple, R. A. (1991). *Water Wave Mechanics for Engineers and Scientists*. Advanced Series on Ocean Engineering - Volume 2. World Scientific Publishing Co Pte. Ltd.

Dohmen-Janssen, C. M. and Hanes, D. M. (2002). "Sheet flow dynamics under monochromatic nonbreaking waves." *Journal of Geophysical Research: Oceans*, 107(C10), 13–1–13–21 3149.

Dohmen-Janssen, C. M., Hassan, W. N., and Ribberink, J. S. (2001). "Mobile-bed effects in oscillatory sheet flow." *J. Geophys. Res.*, 106(C11), 27103–27115.

Fredsøe, J., Anderson, O. H., and Silberg, S. (1985). "Distribution of suspended sediment in large waves.." *J. of Waterway, Port, Coastal end Ocean Eng.*, 111, 1041–1059.

Fuhrman, D., Dixen, M., and Jacobsen, N. (2010). "Physically-consistent wall boundary conditions for the k-$\omega$ turbulence model." *Journal of Hydraulic Research*, 48(6), 793–800.

Fuhrman, D. R., Fredsøe, J., and Sumer, B. M. (2009). "Bed slope effects on turbulent wave boundary layers: 2. comparison with skewness, asymmetry, and other effects." *Journal of Geophysical Research: Oceans*, 114(C3).

Fuhrman, D. R., Schløer, S., and Sterner, J. (2013). "Rans-based simulation of turbulent wave boundary layer and sheet-flow sediment transport processes." *Coastal Engineering*, 73(0), 151 – 166.

Holmedal, L. E., Johari, J., and Myrhaug, D. (2013). "The seabed boundary layer beneath waves opposing and following a current." *Continental Shelf Research*, 65(0), 27 – 44.

Holmedal, L. E. and Myrhaug, D. (2009). "Wave-induced steady streaming, mass transport and net sediment transport in rough turbulent ocean bottom boundary layers." *Continental Shelf Research*, 29(7), 911 – 926.

Holmedal, L. E., Myrhaug, D., and Eidsvik, K. J. (2004). "Sediment suspension under sheet flow conditions beneath random waves plus current." *Cont. Shelf Res.*, 24, 2065–2091.

Holmedal, L. E., Myrhaug, D., and Rue, H. (2003). "The sea bed boundary layer under random waves plus current." *Cont. Shelf Res.*, 23(7), 717–750 erratum 1035.

Hsu, T.-J., Jenkins, J. T., and Liu, P. L.-F. (2004). "On two-phase sediment transport: sheet flow of massive particles." *Proc. R. Soc. Lond. A*, 460, 2223–2250.

Kranenburg, W. M., Ribberink, J. S., Schretlen, J. J. L. M., and Uittenbogaard, R. E. (2013). "Sand transport beneath waves: The role of progressive wave streaming and other free surface effects." *Journal of Geophysical Research: Earth Surface*, 118(1), 122–139.

Kranenburg, W. M., Ribberink, J. S., Uittenbogaard, R. E., and Hulscher, S. J. M. H. (2012). "Net currents in the wave bottom boundary layer: On waveshape streaming and progressive wave streaming." *Journal of Geophysical Research: Earth Surface*, 117(F3).

Longuet-Higgins, M. S. (1953). "Mass transport in water waves." *Philosophical Transactions of the Royal Society of London. Series A, Mathematical and Physical Sciences*, 245(903), pp. 535–581.

McAnally, W. H., Friedrichs, C., Hamilton, D., Hayter, E., Shrestha, P., Rodriguez, H., Sheremet, A., Teeter, A., and null null (2007). "Management of fluid mud in estuaries, bays, and lakes. i: Present state of understanding on character and behavior." *Journal of Hydraulic Engineering*, 133(1), 9–22.

Nielsen, P. (1992). *Coastal bottom boundary layers and sediment transport*, Vol. 4. World scientific.

Rajaratnam, N., Katopodis, C., and Mainali, A. (1988). "Plunging and streaming flows in pool and weir fishways." *Journal of Hydraulic Engineering*, 114(8), 939–944.

Ribberink, J., Dohmen-Janssen, C., Hanes, D., McLean, S., and Vincent, C. (2000). *Near-Bed Sand Transport Mechanisms under Waves; A Large-Scale Flume Experiment*. ASCE, Chapter 253, 3263–3276.

Ribberink, J. S. and Al-Salem, A. A. (1995). "Sheet flow and suspension of sand in oscillatory boundary layers." *Coastal Engineering*, 25(3), 205 – 225.

Richardson, J. and Zaki, W. (1954). "Sedimentation and fluidisation." *Trans. Inst. Chem. Eng.*, 32(Supplement), 35 – 53.

Rodi, W. (1993). *Turbulence Models and Their Application in Hydraulics, A state-of-the-art review.* IAHR Monograph series. A. A. Balkema, Rotterdam, Netherlands, third edition.

Ruessink, B. G., Michallet, H., Abreu, T., Sancho, F., Van der A, D. A., Van der Werf, J. J., and Silva, P. A. (2011). "Observations of velocities, sand concentrations, and fluxes under velocity-asymmetric oscillatory flows." *Journal of Geophysical Research: Oceans*, 116(C3).

Ruessink, B. G., van den Berg, T. J. J., and van Rijn, L. C. (2009). "Modeling sediment transport beneath skewed asymmetric waves above a plane bed." *Journal of Geophysical Research: Oceans*, 114(C11).

Scandura, P. (2007). “Steady streaming in a turbulent oscillating boundary layer.” *Journal of Fluid Mechanics*, 571, 265–280.

Schretlen, J., Ribberink, J., and O’Donoghue, T. (2011). “Boundary layer flow and sand transport under full scale surface waves.” *Coastal Engineering Proceedings*, 1(32).

Sui, T., Staunstrup, L. H., Carstensen, S., and Fuhrman, D. R. (2021). “Span shoulder migration in three-dimensional current-induced scour beneath submerged pipelines.” *Coastal Engineering*, 164, 103776.

van der A, D. A., O‘Donoghue, T., Davies, A. G., and Ribberink, J. S. (2011). “Experimental study of the turbulent boundary layer in acceleration-skewed oscillatory flow.” *Journal of Fluid Mechanics*, 684, 251–283.

van Rijn, L. C. (1993). *Principles of sediment transport in rivers, estuaries and coastal seas*. Amsterdam : Aqua Publications Includes bibliographical references.

van Rijn, L. C., Walstra, D.-J. R., and van Ormondt, M. (2007). “Unified view of sediment transport by currents and waves. iv: Application of morphodynamic model.” *Journal of Hydraulic Engineering*, 133(7), 776–793.

Yalin, M. S. and Karahan, E. (1979). “Inception of sediment transport.” *Journal of the Hydraulics Division*, 105(11), 1433–1443.

Yu, X., Hsu, T.-J., and Hanes, D. M. (2010). “Sediment transport under wave groups: Relative importance between nonlinear waveshape and nonlinear boundary layer streaming.” *Journal of Geophysical Research: Oceans*, 115(C2).

Yuan, J. and Madsen, O. S. (2015). “Experimental and theoretical study of wave-current turbulent boundary layers.” *Journal of Fluid Mechanics*, 765, 480–523.

Zyserman, J. A. and Fredsøe, J. (1994). “Data analysis of bed concentration of suspended sediment.” *Journal of Hydraulic Engineering*, 120(9), 1021–1042.

## List of Tables

**TABLE 1.** Physical wave parameters for Figs. (3) and (5). Here $T_p$ is the wave period, h is the flow depth, $k_p$ is the wave number, and R is the wave skewness factor.

| $T_p$ (s) | $k_p h$ | R |
|---|---|---|
| 6 | 1.11 | 0.53 |
| 8 | 0.74 | 0.55 |
| 10 | 0.60 | 0.56 |
| 12 | 0.49 | 0.58 |

**TABLE 2.** Non-dimensional parameter range for waves plus current beneath $2^{nd}$ order Stokes waves with varying grain size diameter for $\theta$= $45^o$, $90^o$ and $135^o$. Here $\Theta_{max}$ is the maximum Shields parameter and $Z_{min}$ is the minimum Rouse number during a wave-cycle and $U_C$ = 0.1 m/s.

| $d_{50}$ mm | $\Theta_{max}$ | $Z_{min}$ |
|---|---|---|
| 0.13 | 1.58-1.68 | 0.51 |
| 0.21 | 1.08-1.14 | 1.04 |
| 0.32 | 0.78-0.82 | 1.64 |

## List of Figures

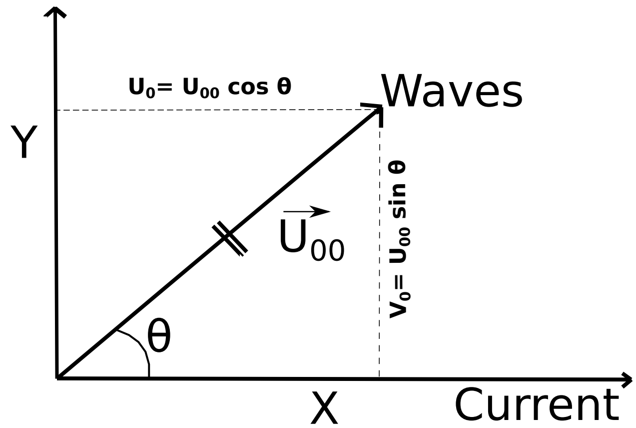


**Fig. 1.** Definition sketch of waves plus current interaction at an angle $\theta$. Here $\mid \vec{U}_{00} \mid = U_{00}$.

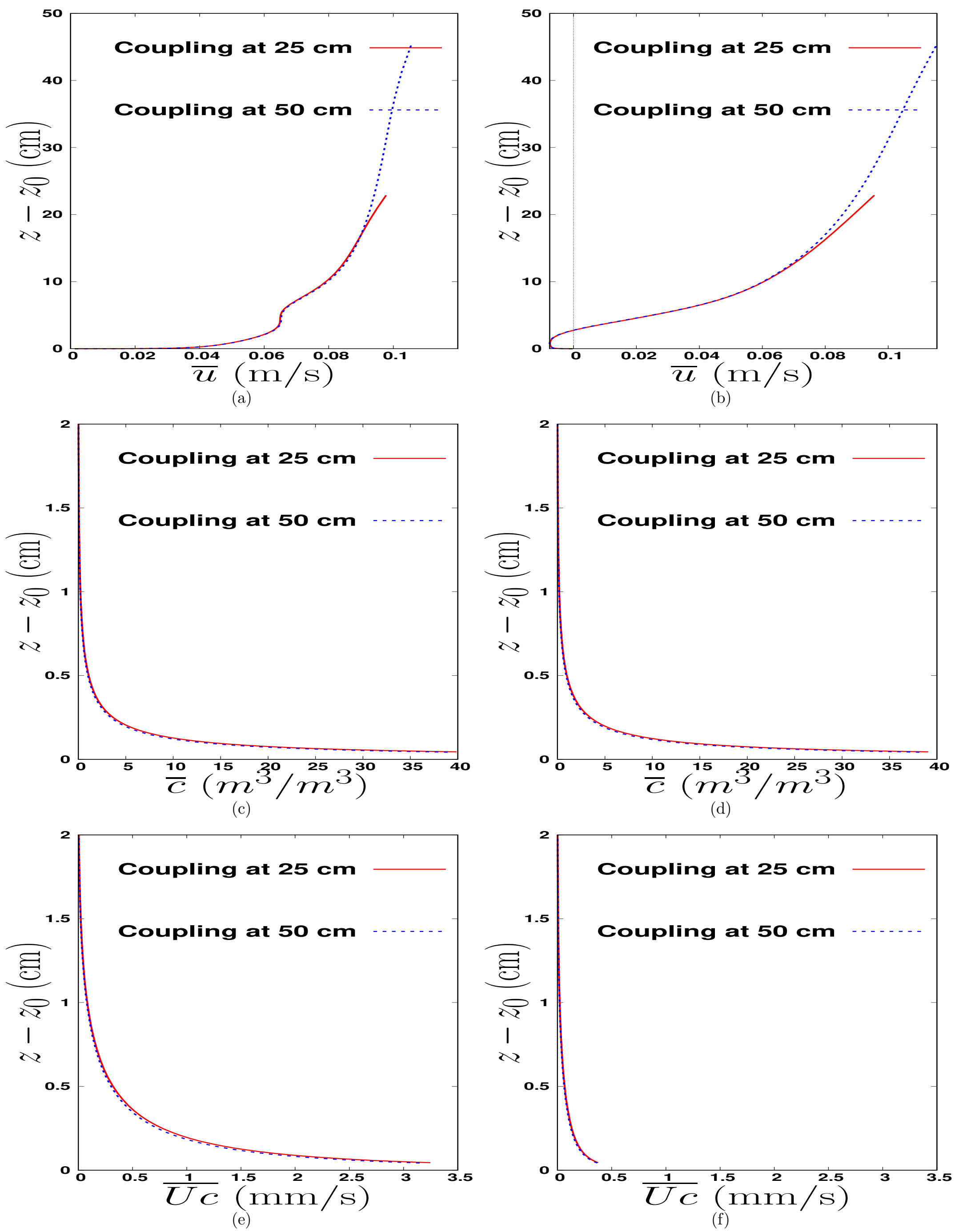


**Fig. 2.** Mean Eulerian velocity profile for (a) waves following the current and (b) waves opposing the current, sediment concentration profiles for (c) waves following the current and (d) waves opposing the current, suspended sediment flux profiles for (e) waves following the current and (f) waves opposing the current.

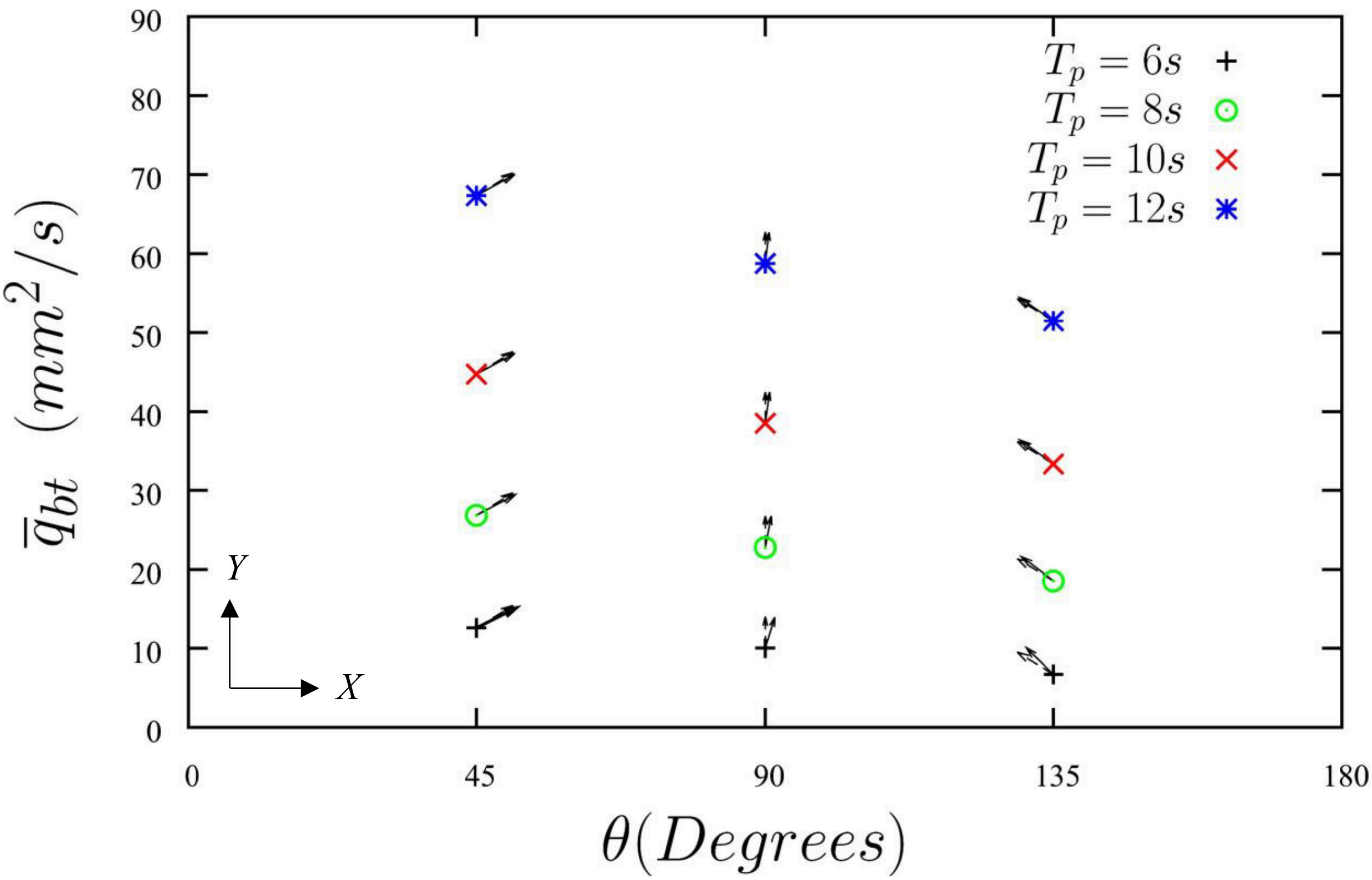


**Fig. 3.** The wave-averaged bedload transport $\overline{q}_{bt}$ beneath $2^{nd}$ order Stokes waves for different angles $\theta$, and four different wave periods $T_p$.

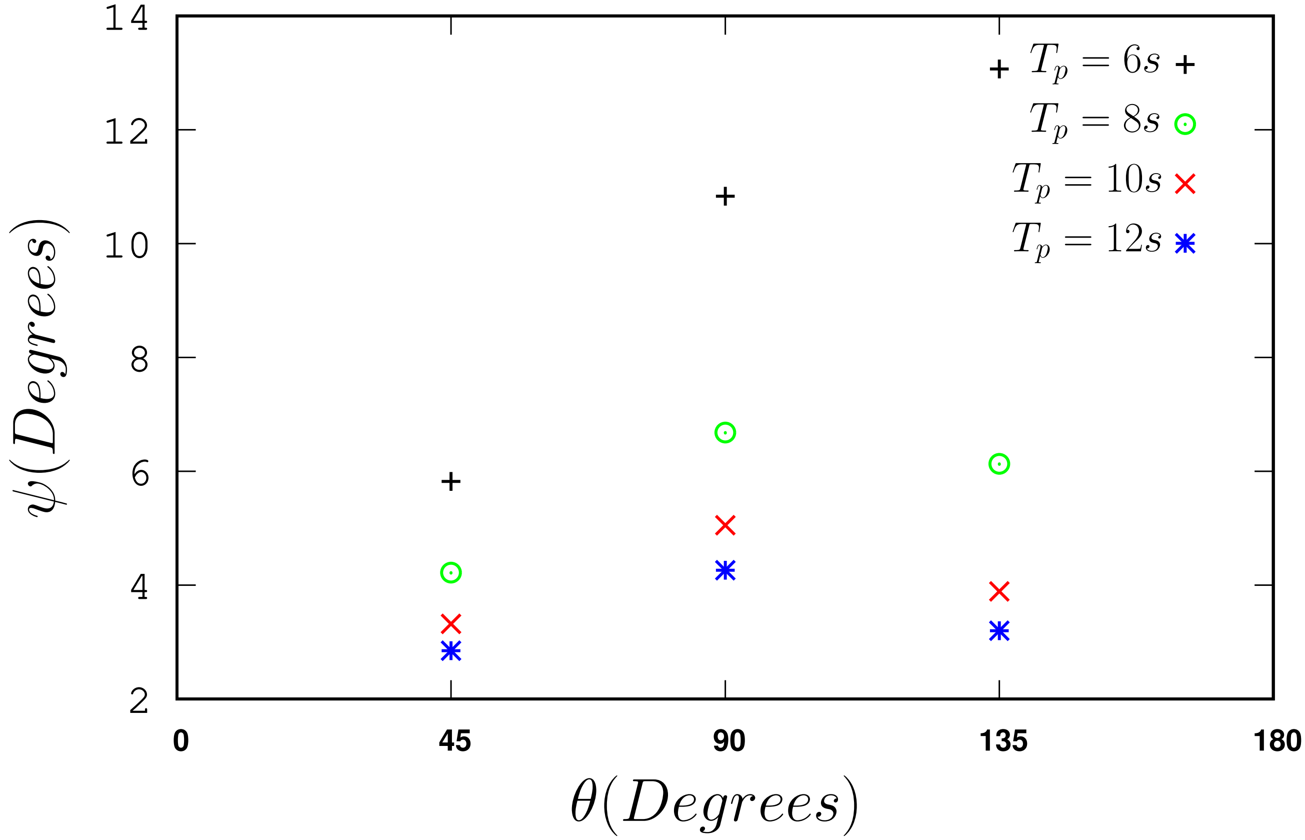


**Fig. 4.** Degree of rotation $\psi$ of the direction of bedload transport from the wave propagation direction beneath $2^{nd}$ order Stokes waves for different angles $\theta$, and four different wave periods $T_p$.

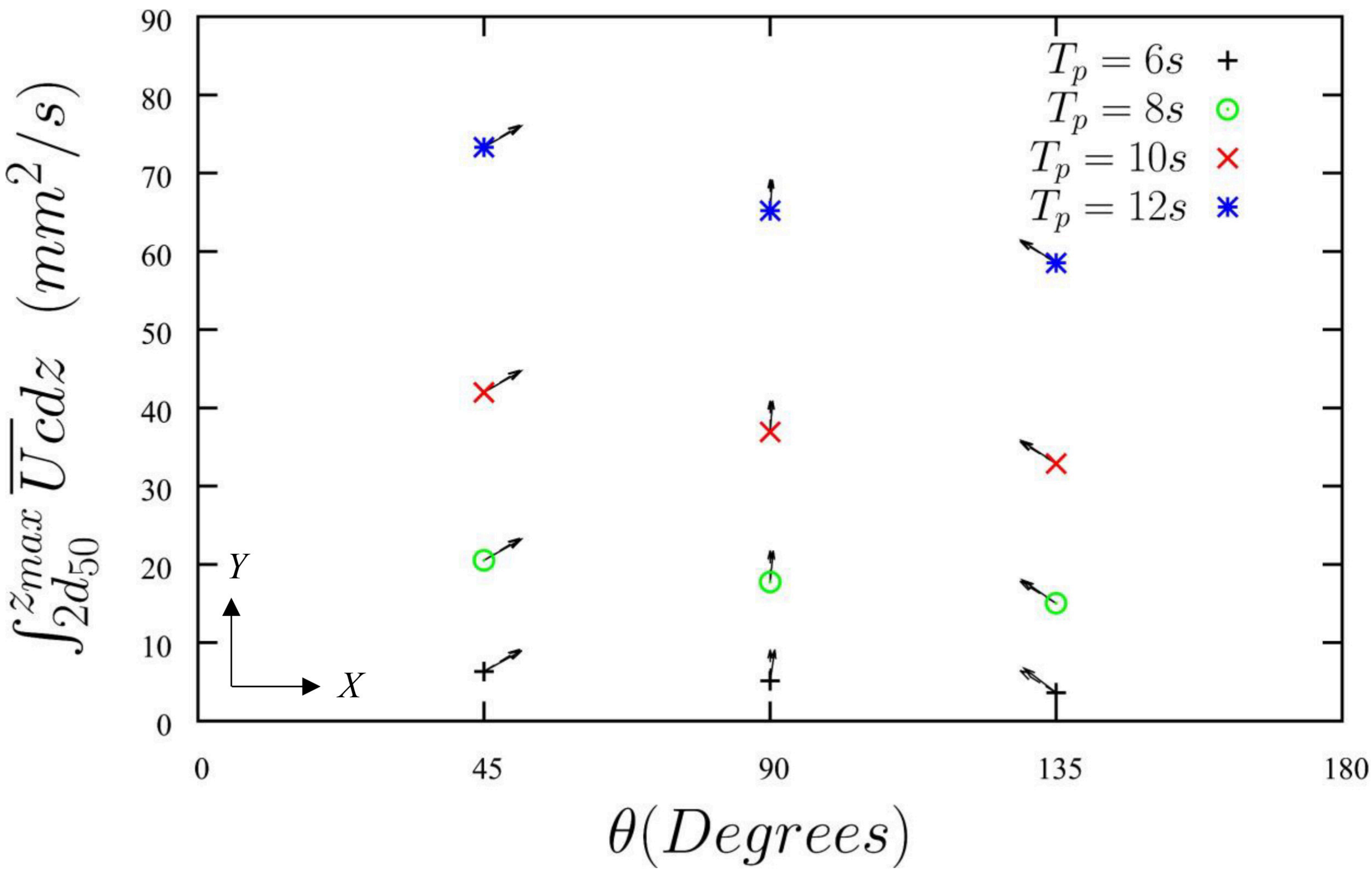


**Fig. 5.** The wave-averaged suspended sediment transport $\int_{2d_{50}}^{z_{max}} \overline{Uc}dz$ beneath $2^{nd}$ order Stokes waves for different angles $\theta$, and four different wave periods $T_p$.

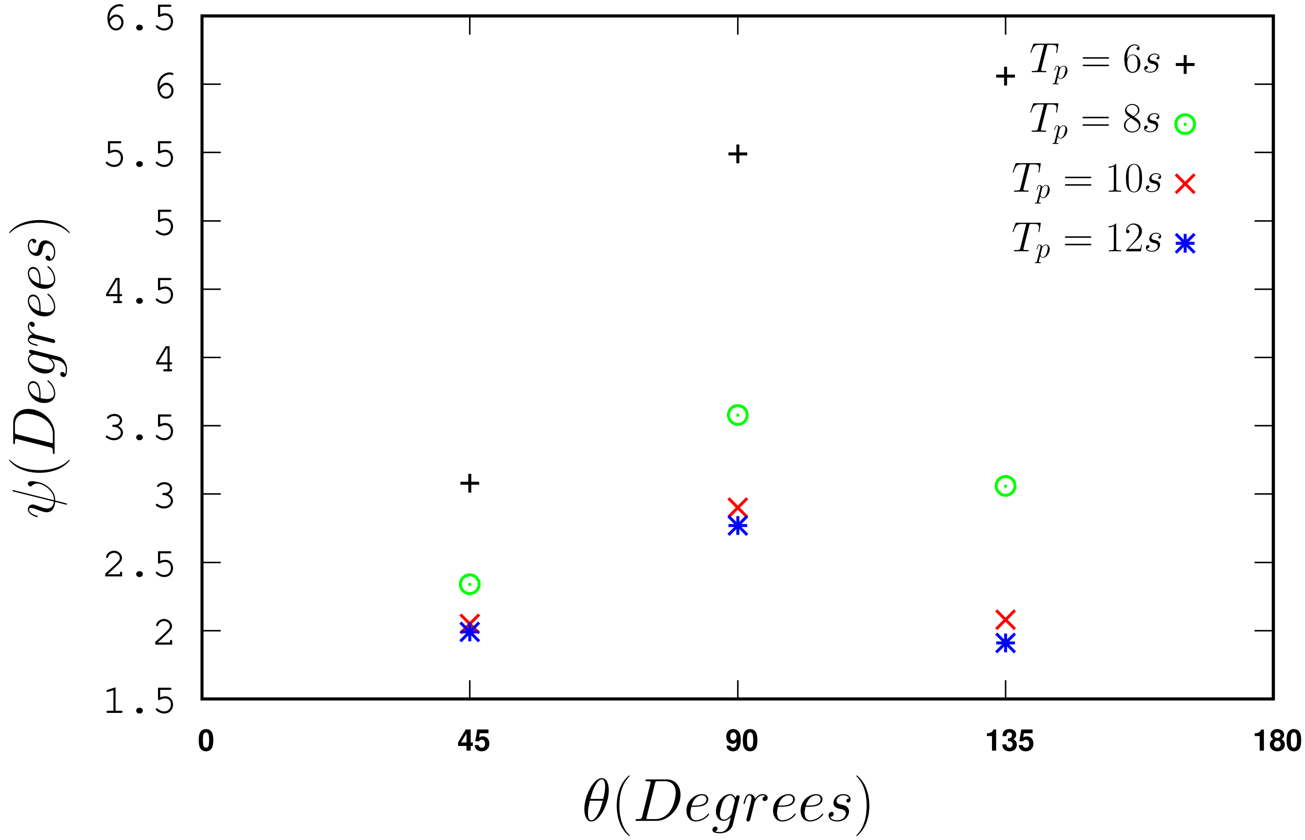


**Fig. 6.** Degree of rotation $\psi$ of the direction of wave-averaged suspended sediment transport from the wave propagation direction beneath $2^{nd}$ order Stokes waves for different angles $\theta$, and four different wave periods $T_p$.

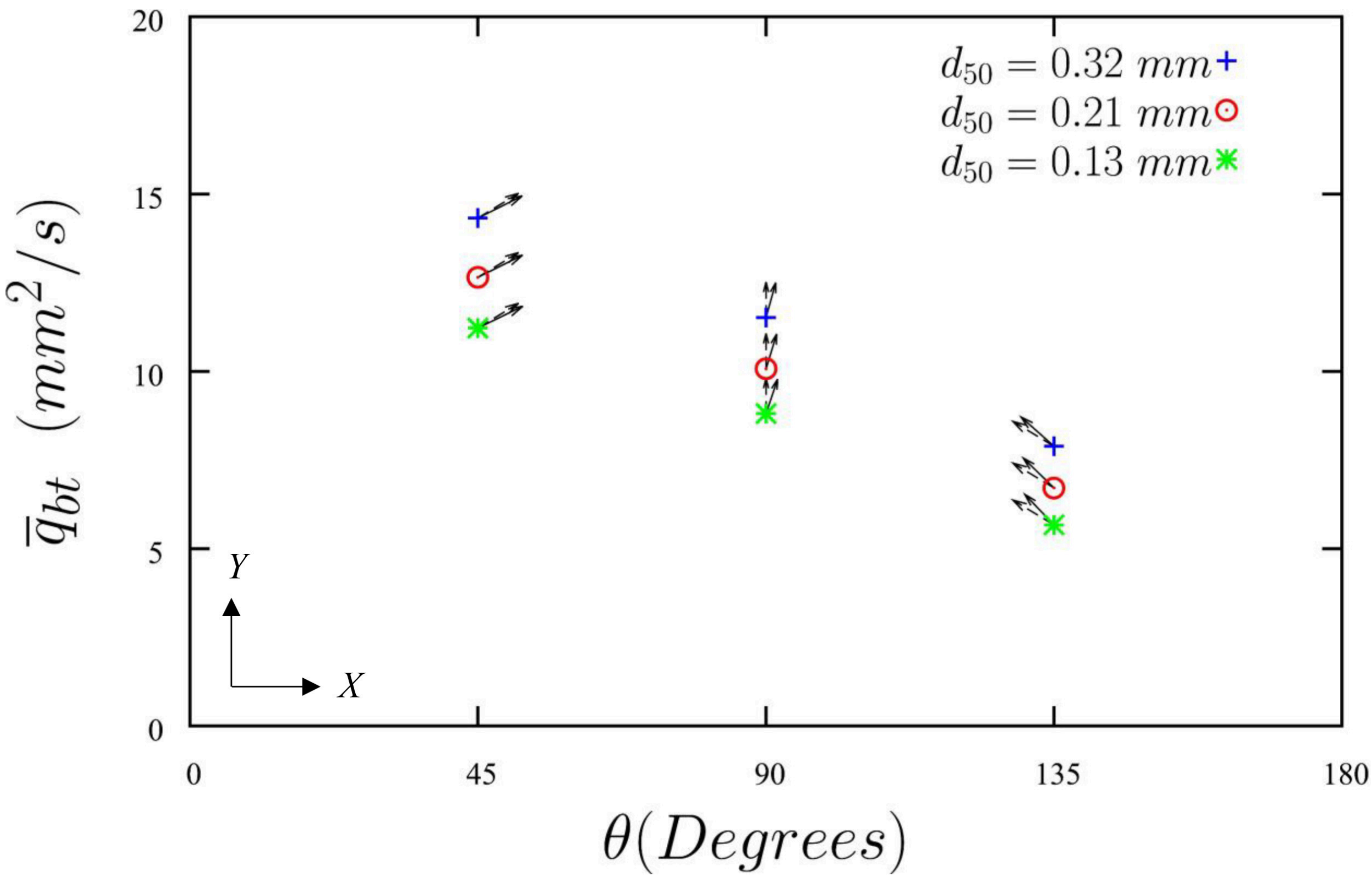


**Fig. 7.** The wave-averaged bedload transport $\overline{q}_{bt}$ beneath $2^{nd}$ order Stokes waves for different angles $\theta$, and three different median grain diameters $d_{50}$.

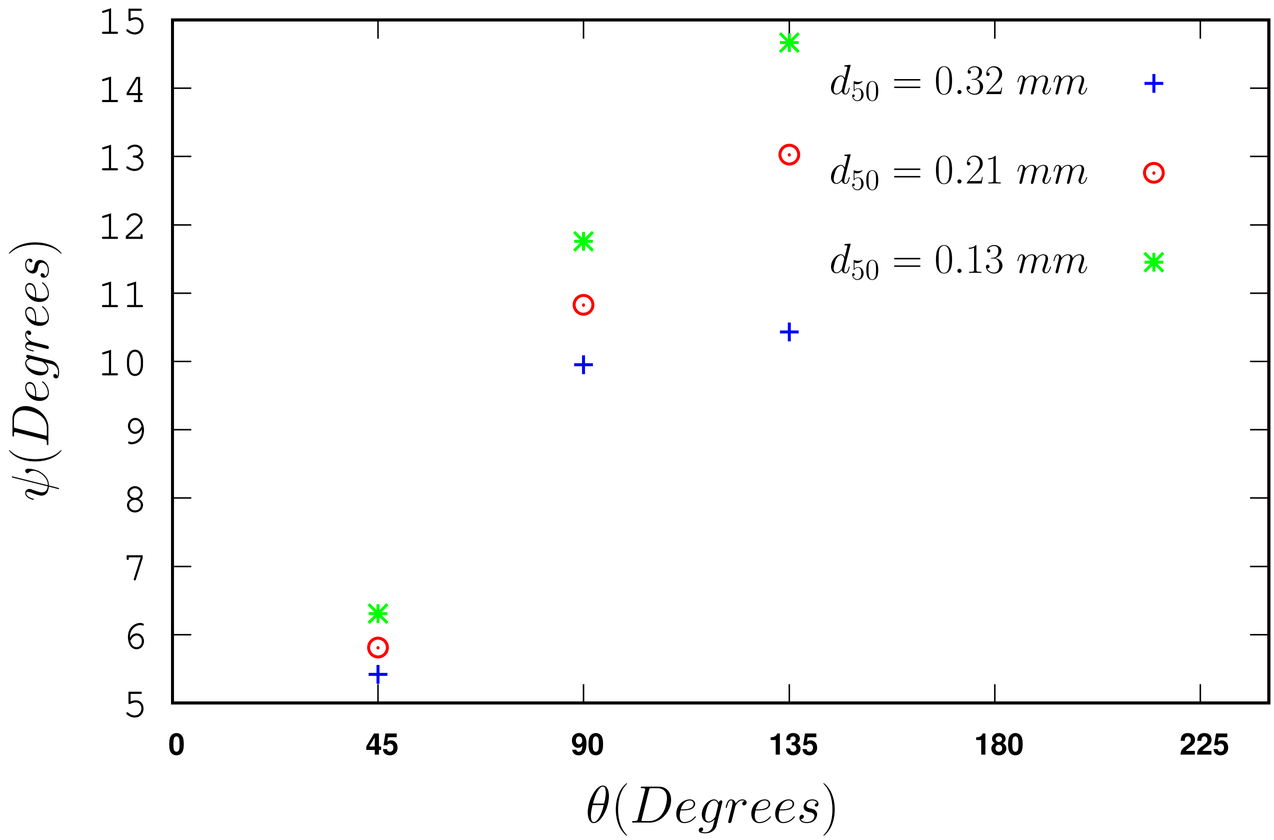


**Fig. 8.** Degree of rotation $\psi$ of the direction of bedload transport from the wave propagation direction beneath $2^{nd}$ order Stokes waves for different angles $\theta$, and three different median grain diameters $d_{50}$.

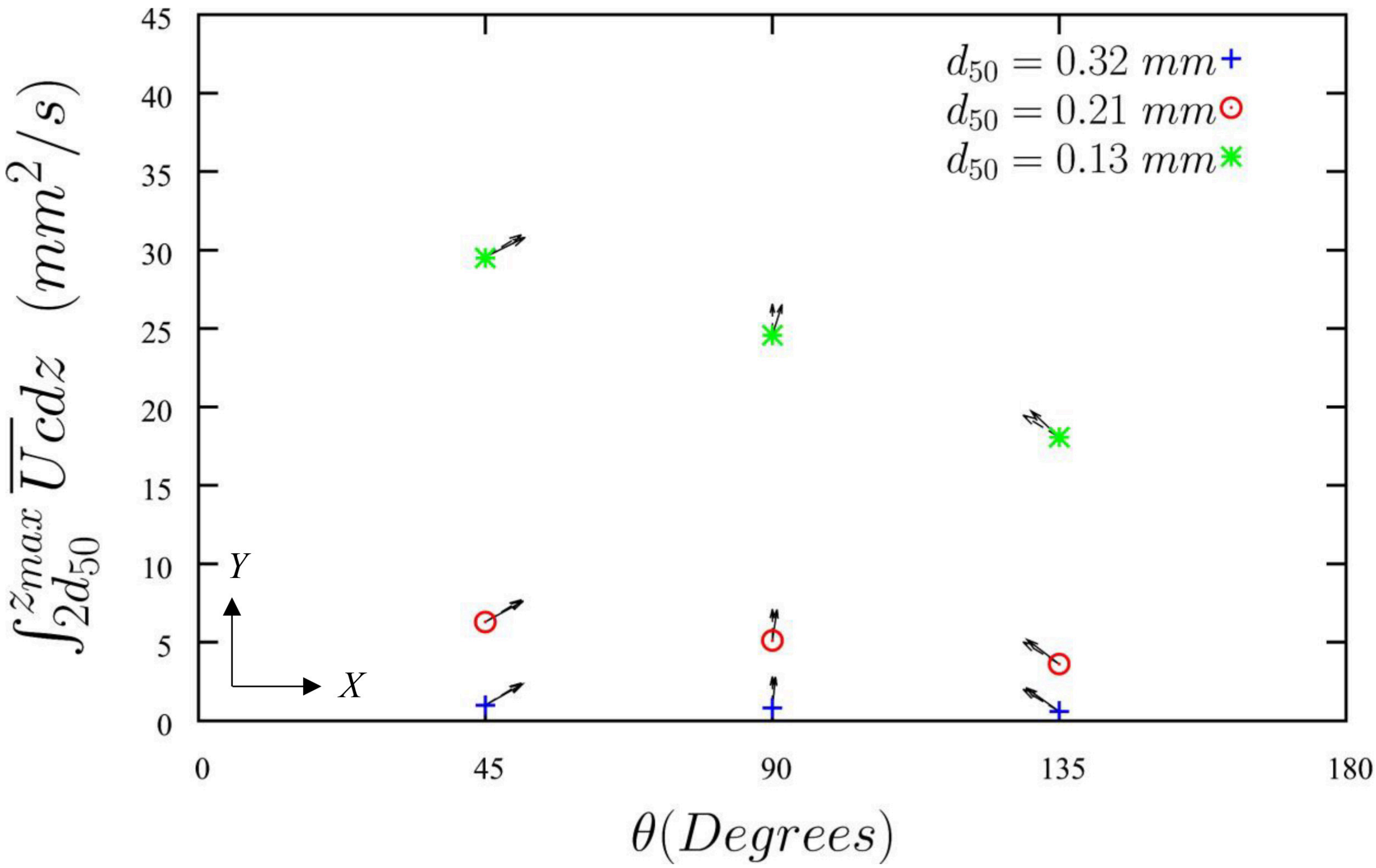


**Fig. 9.** The wave-averaged suspended sediment transport $\int_{2d_{50}}^{z_{max}} \overline{Uc}dz$ beneath $2^{nd}$ order Stokes waves for different angles $\theta$, and three different median grain diameters $d_{50}$.

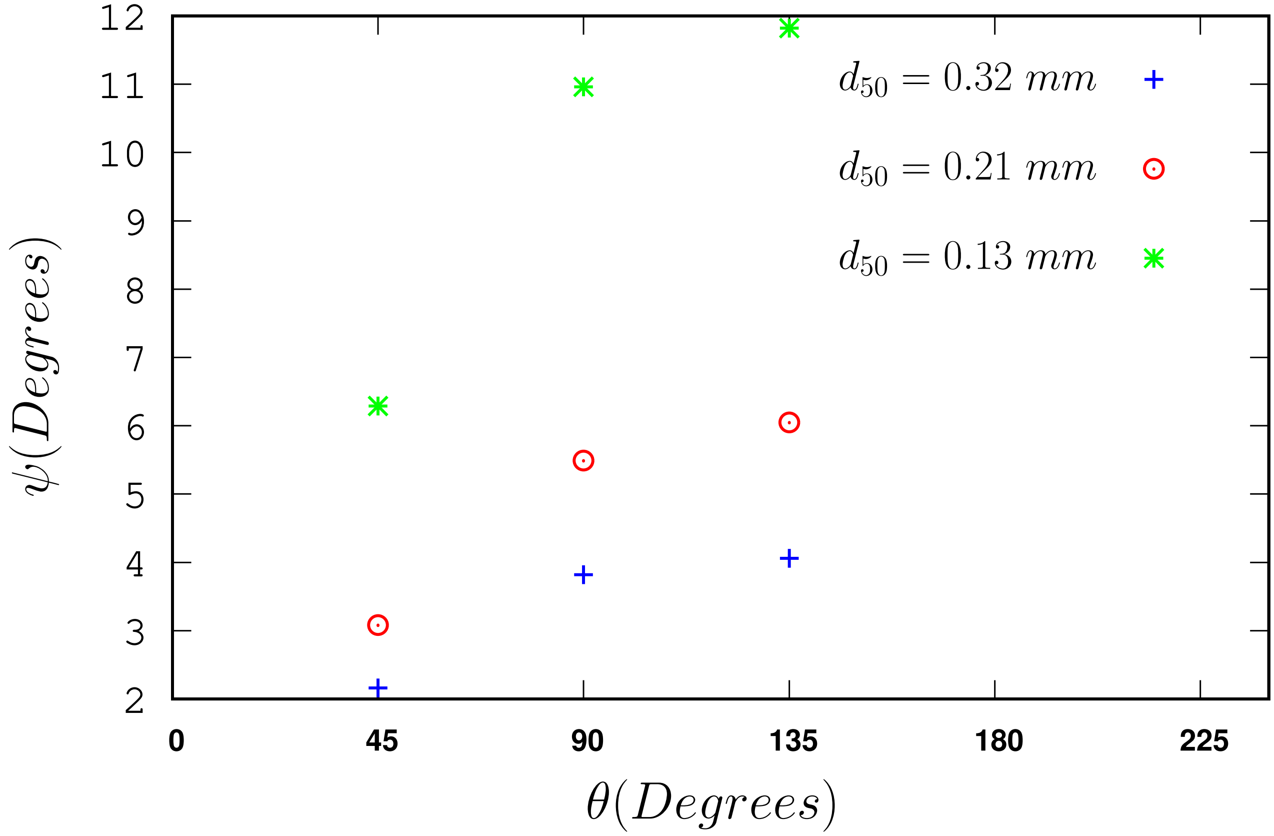


**Fig. 10.** Degree of rotation $\psi$ of the direction of wave-averaged suspended sediment transport from the wave propagation direction beneath $2^{nd}$ order Stokes waves for different angles $\theta$, and three different median grain diameters $d_{50}$.